RSC Advances

RSC Publishing

PAPER

Tuning the properties of an anthracene-based PPE-PPV copolymer by fine variation of its macromolecular parameters

Cite this: *RSC Advances*, 2013, **3**, 6972

Francesca Tinti,[a] Fedlu K. Sabir,[ab] Massimo Gazzano,[a] Sara Righi,[c] Christoph Ulbricht,[d] Özlem Usluer,[d] Veronika Pokorna,[e] Vera Cimrova,[e] Teketel Yohannes,[b] Daniel A. M. Egbe*[d] and Nadia Camaioni*[a]

Received 20th November 2012,
Accepted 18th February 2013

DOI: 10.1039/c3ra22967j

www.rsc.org/advances

The effects of a moderate variation of the molecular weight on the optical, structural, morphological and transport properties of an anthracene-containing PPE-PPV copolymer are investigated, as well as their overall implication on the photovoltaic parameters of bulk-heterojunction solar cells. Just a two-fold variation in the molecular weight is enough to induce appreciable changes in the properties of the investigated polymer films, indicating that a fine tuning of the macromolecular parameters is required for the optimization of the properties of polydispersed molecular systems. A remarkable role of the polydispersity index in the organization of polymer chains, thus reflecting in the electronic properties of the polymer films, is observed.

1. Introduction

Soluble π-conjugated polymers have attracted increasing interest in the last years, because of the unique combination of solution-processability, robust mechanical properties, and tunability of their electronic properties, making these innovative semiconducting materials excellent candidates for large-area, cost-effective and high throughput production of flexible electronics.[1,2]

The electronic properties of conjugated polymers are not simply dependent on their chemical structure but are highly affected by regioregularity and macromolecular parameters, such as molecular weight (MW) and polydispersity index (PDI), so the advantages of monodisperse low molecular weight conjugated molecules over polymers are often underlined.[3,4] Macromolecular parameters are known to have great effects on the optical and charge transport properties of conjugated polymer films, also through a different organization of polymer chains in the solid state induced by different MW.[5,6]

Considerable amount of work has been reported in the literature on the effect of MW on the properties of conjugated polymers. Most of these studies have been carried out on regioregular poly(3-hexylthiophene) (P3HT), a model conjugated polymer widely used in the fabrication of organic field-effect transistors and solar cells.[7] Charge carrier mobility in P3HT films is usually found to increase with MW,[8–10] though an opposite behaviour has been also reported.[11] This discrepancy could be explained by different morphologies of the investigated P3HT films, likely due to different deposition conditions. More frequently the overall crystallinity of P3HT films decreases with increasing MW,[5,6,8,10] however it is believed that charge trapping processes at the boundaries of the crystalline grains observed at low MW could be responsible for the poor transport properties.[8] Consequently, the combined effect of MW on charge transport properties and chain packing of P3HT reflects on the performance of P3HT:PCBM (PCBM is [6,6]-phenyl-C_{61}-butyric acid methylester) solar cells, as well as on the optimum annealing temperature required to induce the optimum inter-mixing between the photovoltaic blend components and leading to the highest efficiency.[11–14] Improved charge carrier mobility for high molecular weight has also been observed with conjugated polymers different from P3HT[15,16] and it is nowadays ascertained that high MW is required for good charge transport properties as well as for good solar cell performance.

Concerning PDI, systematic studies of its effect on the electronic properties of conjugated polymers are lacking, however it is common thinking that a narrow distribution of

[a]*Istituto per la Sintesi Organica e la Fotoreattività, Consiglio Nazionale delle Ricerche, via P. Gobetti 101, I-40129 Bologna, Italy. E-mail: nadia.camaioni@isof.cnr.it*
[b]*Department of Chemistry, University of Addis Ababa, P.O. Box 1176, Addis Ababa, Ethiopia*
[c]*Laboratorio di Micro e Submicro Tecnologie Abilitanti per l'Emilia Romagna (MIST E-R S.C.R.L.), via P. Gobetti 101, 40129 Bologna, Italy*
[d]*Linz Institute for Organic Solar Cells (LIOS), Johannes Kepler University Linz, Altenbergerstr. 69, 4040 Linz, Austria. E-mail: daniel_ayuk_mbi.egbe@jku.at*
[e]*Institute of Macromolecular Chemistry, Academy of Sciences of the Czech Republic, Heyrovsky Sq. 2, 16206 Prague 6, Czech Republic*

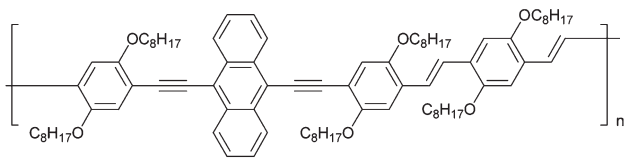

AnE-PV*stat*

Scheme 1 Chemical structure of AnE-PV*stat* (octyl = C_8H_{17} and 2-ethylhexyl = C_8H_{17} side-chains are randomly distributed).

molecular weights could be more advisable for high performance polymers.

In this paper, we report the effects of a moderate variation of the macromolecular parameters of an anthracene-containing poly(*p*-phenylene-ethynylene)-alt-poly(*p*-phenylene-vinylene) (PPE-PPV), having randomly distributed linear octyl and branched 2-ethylhexyl side chains, denoted AnE-PV*stat* (Scheme 1). Light-emitting diodes showing a turn-on voltage below 2 V (ref. 17) and solar cells exhibiting a state-of-art efficiency for PPV-based materials of around 5% have been already demonstrated by using AnE-PV*stat*,[18] as well as its very good ambipolar charge transport properties.[19] AnE-PV*stat* has already proven to be the best material among a series of 13 anthracene-containing PPE-PPV copolymers, denoted AnE-PVs, which are characterized by the same conjugated backbone, but different combinations of grafted alkoxy side-chains. Both side-chain-based well-defined[20–22] and side-chain-based statistical AnE-PVs[17,23,24] have been synthesized and thoroughly investigated so far. Number-average molecular weights (M_n) between 7000 and 70 000 g mol^{-1}, with PDI between 1.9 and 5.0, have been obtained for the 13 soluble AnE-PVs reported up to now.[17,20,21,23] High PDI are consistent with the Horner–Wadsworth–Emmons polycondensation route, however it can be reduced through a post-polycondensation treatment, such as extraction of the crude product with hot diethylether, which helps to keep PDI below or around 2.[25] In the case of side-chain-based well-defined copolymers, the grafting of linear alkoxy side-chains on phenylenes close to the anthracence unit is crucial to enable molecular ordering, as revealed by X-ray scattering and photophysical studies.[21,22] Of the six already reported side-chain-based statistical AnE-PVs, only AnE-PV*stat* shows ordering.[17,22]

Differently from other works, considering wide ranges of MW, with values of the number-average molecular weight from a few to tens or hundreds of kg mol^{-1} and resulting in significant variations of polymer properties, in this study the effects on the optical, structural, morphological and transport properties of AnE-PV*stat* films due to a moderate variation of the molecular weight are investigated. Only AnE-PV*stat* samples with high MW are here considered (M_n of the order of 10^4 g mol^{-1}), more promising for electronic applications, and it is shown that relevant effects are observed even with a variation of MW of about twice. More interestingly, it is demonstrated that the behaviour of charge carrier mobility with the applied field is affected by the macromolecular parameters in AnE-PV*stat* films, being the mobility trend with field rarely considered in this kind of studies. In addition, the comparison of two polymer samples with comparable MW but different polydispersity index clearly shows the crucial role of PDI in the organization of polymer chains, with better properties for the sample with higher PDI and contrary to the common thinking. Finally, the effect of the properties of the investigated polymer samples on the photovoltaic parameters of bulk-heterojunction solar cells is also considered.

2. Experimental

Gel permeation chromatography (GPC)

GPC measurements were performed using Pump Deltachrom (Watrex Comp.), autosampler Midas, with two columns PL gel MIXED-B LS, particle size 10 μm. Evaporative light scattering detector PL-ELS-1000 (Polymer Laboratories) was used; THF was the mobile phase. Polystyrene standards were used for calibration.

Optical characterization

Absorption and photoluminescence spectra were carried out on dilute chloroform solutions (4×10^{-7} mol L^{-1}) and on thin films spin-coated (1000 rpm) from chlorobenzene solutions (10 g L^{-1}) onto quartz substrates. The film thickness, measured with a Tencor AlphaStep profilometer, was the same for the three polymers samples (55 nm). The solutions prepared for spin-coating deposition were stirred for 4 days at 45–50 °C before using. After the spin-coating deposition, the films were solvent-vapor annealed (chlorobenzene) overnight. Absorption and photoluminescence spectra were recorded with a Perkin Elmer 950 spectrophotometer and a Spex Fluorolog II 1681 spectrofluorometer, respectively.

X-Ray diffraction (XRD)

AnE-PV*stat* films for XRD investigation were drop-casted onto quartz substrates from chlorobenzene solutions (30 g L^{-1}), stirred for 4 days at 45–50 °C. After the deposition, the films were solvent-vapor annealed (chlorobenzene) overnight. X-ray diffraction analysis was carried out by means of a PANalytical X′Pert diffractometer equipped with a copper anode (λ_{mean} = 0.15418 nm) and a fast X′Celerator detector. Step 0.05° (2θ), counting time 120 s/step. Mineral quartz 'zero background' sample holders (The Gem Dugout, State College, PA-USA) were used in order to strongly minimize support contribution to the total scattering. The films were directly investigated in reflection geometry. The domain length was calculated by the Scherrer equation[26] from parameters of the peak at 5.8° (2θ).

Atomic force microscopy (AFM)

AFM imaging was performed under ambient conditions using a commercial atomic force microscope (NanoScope Dimension IIIa, MultiMode Digital Instruments, Santa Barbara, CA, USA) in tapping mode. Tapping mode etched silicon probes OTESPA (Veeco Instrument) with aluminium reflective coating on the backside of the cantilever were used (cantilever resonance

frequencies about 300 kHz, a typical spring constant 42 N m^{-1}, the tip radius of about 7 nm). The analysis of AFM images was performed with the NANOSCOPE software (Digital Instruments, Inc.). The AnE-PV*stat* films for AFM inspection were drop-casted onto glass substrates covered with indium–tin–oxide from chlorobenzene solutions (30 g L^{-1}), which were stirred for 4 days at 45–50 °C. After the deposition, the films were solvent-vapor annealed (chlorobenzene) overnight.

Time of Flight (TOF) measurements

AnE-PV*stat* films were drop-casted onto Al-coated quartz substrates from chlorobenzene solutions (30 g L^{-1}), stirred for 4 days at 45–50 °C. After the deposition, the films were solvent-vapor annealed (chlorobenzene) overnight. The device structure was completed with a vacuum evaporated semitransparent aluminium electrode (20 nm), acting as the illuminated electrode. The device area was 0.25 cm^2 and the film thickness 7.8, 4.2, and 3.6 μm for AnE-PV*stat*-a, AnE-PV*stat*-b, and AnE-PV*stat*-c, respectively. A nitrogen laser (λ = 337 nm) with a pulse duration of 6–7 ns was used to photogenerate charge carriers. The absorption coefficient at the excitation wavelength was found to be between 2.34 × 10^4 cm^{-1} and 2.97 × 10^4 cm^{-1} for the three polymer samples, so most of light was absorbed within the first 300–400 nm of the investigated films. A variable DC potential was applied to the samples and, in order to ensure a uniform electric field inside the device, the total photogenerated charge was kept less than $0.1CV$ (where C is the sample capacitance and V the applied potential) by attenuating the laser beam intensity with quartz neutral filters. The photocurrent was monitored across a variable load resistance by using a Tektronix TDS620A digital oscilloscope. TOF measurements were performed at room temperature and under dynamic vacuum (10^{-5} mbar).

Solar cells

Solar cells were fabricated on patterned ITO-coated glass substrates, previously cleaned in detergent and water, and then ultrasonicated in acetone and isopropyl alcohol for 15 min each. A PEDOT:PSS (Clevios P VP AI 4083) layer was spin-coated at 4000 rpm onto UV-ozone-treated ITO-coated substrates to a thickness of around 40 nm, then baked in an oven at 140 °C for 10 min. AnE-PV*stat* polymer samples were blended with PCBM (Aldrich) and dissolved in chlorobenzene (17 g L^{-1}). The solutions were stirred at 40 °C overnight. The blend solutions were spin-coated at 500 rpm in air onto the ITO/PEDOT:PSS substrates. The spin-coated blends were solvent-vapor annealed (chlorobenzene) for one hour before transferring to an argon glove-box, where the device structure was completed with the thermal evaporation of the LiF (0.9 nm)/Al (80 nm) electron-collecting contact at a base pressure of 3 × 10^{-6} mbar. The active device area, defined by the shadow mask used for the top contact deposition, was 8 mm^2. The thickness of the active layer was 135 nm, 130 nm and 93 nm for solar cells based on AnE-PV*stat*-a, AnE-PV*stat*-b, and AnE-PV*stat*-c, respectively.

The electrical characterization was carried out in glove-box at room temperature. Solar cells were illuminated by using a solar simulator (SUN 2000 Abet Technologies, AM1.5G) and the light power intensity was calibrated using a certified silicon solar cell. The current–voltage curves were taken with a Keithley 2400 source-measure unit.

3. Results and discussion

Three AnE-PV*stat* samples, here identified as AnE-*PVstat-a*, AnE-PV*stat*-b and AnE-PV*stat*-c, were prepared for this study. The three polymers were synthesized through a well established procedure,[23] involving the Horner–Wadsworth–Emmons olefination reaction to polycondensate equimolar amounts of both dialdehydes and both bisphosphonate esters shown in Scheme 1.[21] Different values of the macromolecular parameters were obtained by changing the stirring speed during the reaction and the extraction method. The values of number-average molecular weight, the weight-average molecular weight (M_w) and the polydispersity index of the three AnE-PV*stat* samples under study, obtained by gel permeation chromatography, are collected in Table 1. M_w value for AnE-PV*stat*-b was nearly two times lower than that determined for AnE-PV*stat*-a and AnE-PV*stat*-c. In addition, as shown by the GPC curves (Fig. 1), AnE-PV*stat*-a exhibited a broader MW distribution compared with AnE-PV*stat*-c.

The optical properties of the three polymer samples were investigated by UV-Vis absorption and photoluminescence (PL) spectroscopy, both in dilute solutions and in thin films spin-coated onto quartz substrate (Fig. 2). As expected, no meaningful differences were observed in the optical spectra of dilute solutions, showing the same spectral features already reported for AnE-PV*stat*,[23] with the same emission peak position (579 nm) and very close absorption maxima at 548, 547 and 543 nm for AnE-PV*stat*-a, AnE-PV*stat*-a and AnE-PV*stat*-c, respectively. Films of AnE-PV*stat* spin-cast from chlorobenzene solution are known to show a stacking behaviour,[23] resulting in structured absorption and photoluminescence spectra exhibiting two peaks, as shown in Fig. 2b for the AnE-PV*stat* samples here investigated. Given the narrow molar mass range for the three polymer samples, significant variations of the optical spectra were not observed, nevertheless some considerations can be made.

The main difference in the absorption spectra of films is between AnE-PV*stat*-c and the other two samples, the former showing (i) the lower energy peak slightly blue-shifted (located

Table 1 Macromolecular and XRD parameters of the three polymer samples here investigated: number-average molecular weight M_n, weight-average molecular weight M_w, polydispersity index PDI, interlayer distance d_i, peak width FWHM, mean domain length L and mean number of interlayer lattice per domain $n_i = L/d_i$

Sample	Macromolecular parameters			XRD parameters			
	M_n (g mol^{-1})	M_w (g mol^{-1})	PDI	d_i (nm)	FWHM (°,2θ)	L (nm)	n_i
AnE-PV*stat*-a	30 600	83 900	2.74	1.50	0.84	10.5	7.0
AnE-PV*stat*-b	18 000	43 700	2.43	1.53	0.67	13.2	8.6
AnE-PV*stat*-c	41 200	82 700	2.01	1.52	0.86	10.3	6.8

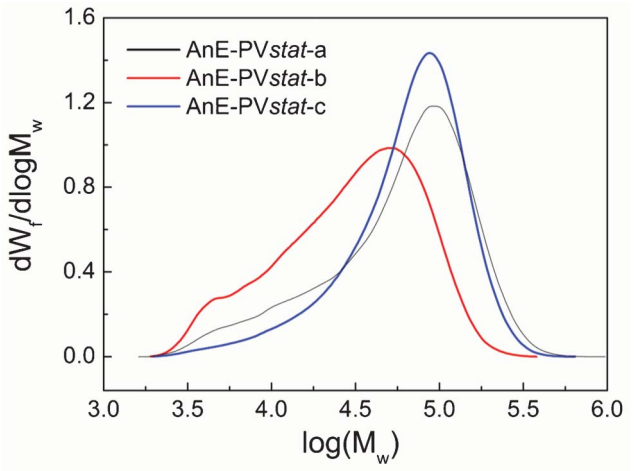

Fig. 1 GPC curves of the three polymer samples: AnE-PV*stat*-a (black), AnE-PV*stat*-b (red) and AnE-PV*stat*-c (blue). THF was the mobile phase. Polystyrene standards were used for calibration.

at 579 nm, against 586 and 588 nm for samples AnE-PV*stat*-a, and AnE-PV*stat*-b, respectively), indicating a moderate reduction of the effective conjugation, and (ii) a different relative intensity of the two absorption peaks (Fig. 2b). These features should not be related to MW, given the comparable molecular weight of AnE-PV*stat*-c and AnE-PV*stat*-a, and could indicate a different molecular organization in the solid state due to the different polydispersity (Table 1).

Concerning the PL spectra, somewhat different emission capability were observed by films showing a comparable absorbance at the excitation wavelength of 450 nm (Fig. 2b), qualitatively indicating the highest luminescence quantum yield for AnE-PV*stat*-c and the lowest for AnE-PV*stat*-a. Again this behaviour can be related to a different strength of π–π interchain interactions in the three samples, leading to a quenching of emission.[25]

The preliminary indications on the solid state organization of the three samples were confirmed by X-ray diffraction experiments, conducted on films drop-cast from chlorobenzene solutions. The diffraction patterns shown in Fig. 3 are characterized by a sharp intense reflection at low angle, due to interlayer stacking, and by a wide band with no resolved peaks at high angle. The interlayer distance (d_i) and the mean domain length (L), determined from the peak parameters of the XRD patterns, are displayed in Table 1. The distance between the planes shows only a slight variation in the three polymer samples, with a modest lengthening on lowering the molar mass. On the contrary, the domain length seems to be strongly dependent on M_n and M_w. Indeed, the AnE-PV*stat*-b sample, characterized by the lowest molecular mass parameters, displays an increase of L of about 30% with respect to the other samples and a corresponding increase of the number of lattice planes per domain (n_i).

A rough evaluation of the ratio of the area of the main peak to that the overall area under the XRD profile suggests that the overall order degree of the investigated polymer films follows

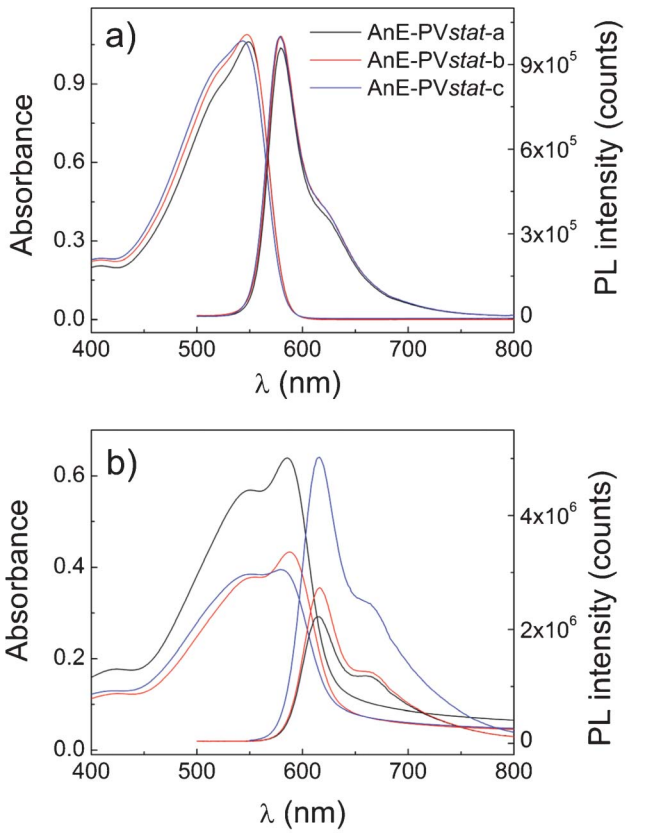

Fig. 2 Absorption (left) and photoluminescence (right) spectra in normalized scales of a) dilute solutions and b) thin films of the same thickness (55 nm) spin-cast onto quartz substrate. The excitation wavelength was 400 nm for solutions and 450 nm for films.

the order: AnE-PV*stat*-a > AnE-PV*stat*-b > AnE-PV*stat*-c. However, if the number of lattice planes per domain is considered, AnE-PV*stat*-b results in the sample with the largest ordered domains. The comparison of the XRD patterns of samples AnE-PV*stat*-a and AnE-PV*stat*-c, roughly showing the same peak in the GPC curves but different PDI, suggests that polydispersity plays an important role in polymer chains organization.

The atomic force microscopy inspection of films deposited under the same condition used for the XRD investigation revealed a close correlation between the macromolecular parameters and the film topology (Fig. 4). Polymer chains in AnE-PV*stat*-b film, with the lowest MW, were able to pack in smaller domains, compared with the samples with higher molar mass, while a prevailing fibril-like formation was observed for samples AnE-PV*stat*-a and AnE-PV*stat*-c. The smaller-domain morphology of AnE-PV*stat*-b film was also accomplished by a higher root-mean-square roughness (R_q), compared to the films made of the polymers with higher molecular weight. The values of R_q evaluated on a scan area of 0.5 μm × 0.5 μm were 1.34, 1.58 and 0.71 nm for AnE-PV*stat*-a, AnE-PV*stat*-b and AnE-PV*stat*-c, respectively, and maintained the same trend over a larger scan area of 1.0 × 1.0 μm. By comparing AnE-PV*stat*-a, AnE-PV*stat*-c, exhibiting a similar

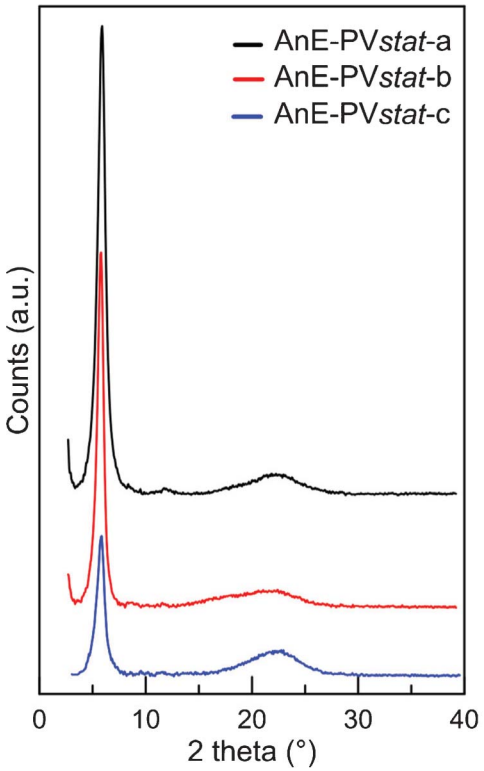

Fig. 3 XRD patterns of films drop-cast from chlorobenzene solutions onto quartz holder.

MW, the lower R_q was observed for the one showing the lower polydispersity, indicating that the distribution of molecular weight plays a role in the film morphology.

The comparison of Fig. 4a and 4c shows the effect of the different polydispersity index on the film morphology. Indeed, the higher PDI of AnE-PV*stat*-a seems to be beneficial for a more regular arrangement of polymer chains, confirming the XRD data, and as previously suggested for poly(3-alkylthiophenes).[12]

The drift mobility (μ) of charge carriers in films of AnE-PV*stat* was investigated as a function of the electric field (E) by using differential small-signal Time of Flight,[27] considered a ''direct'' method for the investigation of bulk transport properties in disordered materials. The TOF experiments were performed on sandwich-type devices with the structure Al/AnE-PV*stat*/Al, where the polymer layer was drop-casted from the same chlorobenzene solutions used for the preparation of the XRD and AFM samples. The sign of charges generating the photocurrent signals was selected by appropriately biasing the devices.

The photocurrent transients for the three polymer samples are displayed in a double-logarithmic representation in Fig. 5 for a comparable electric field of about 1×10^5 V cm^{-1}. The shape of TOF signals shown in the figure is representative for transients observed for different values of E and indicates a quite dispersive transport. Transit times of charge carriers

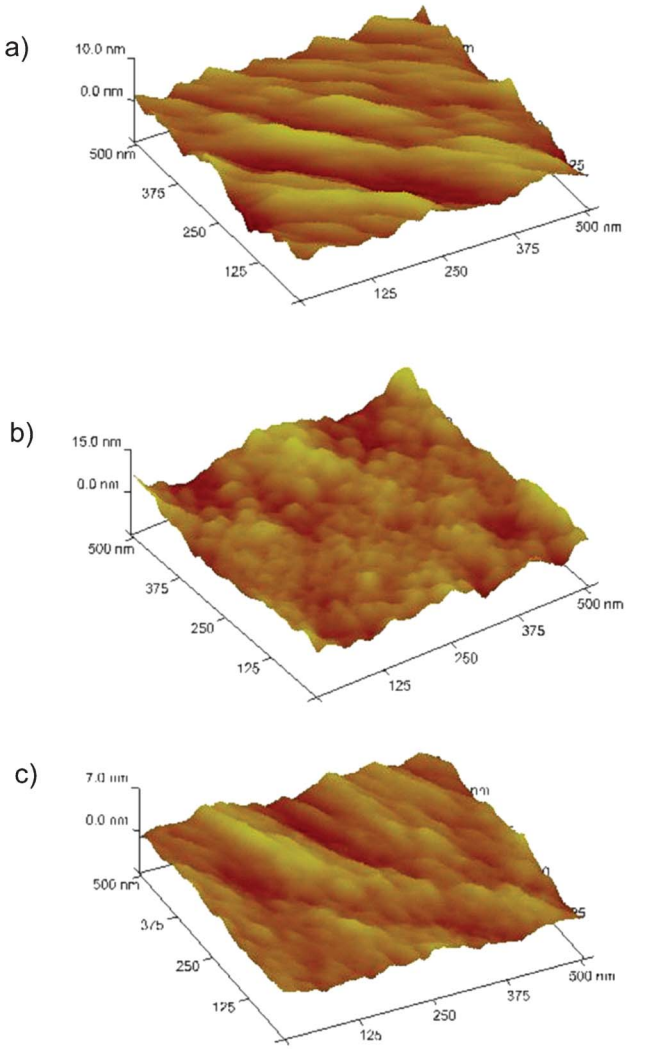

Fig. 4 Three dimensional AFM topography images of drop-casted films made of: a) AnE-PV*stat*-a; b) AnE-PV*stat*-b; c) AnE-PV*stat*-c.

were evaluated with the same method in all cases, that is from the inflection point visible in the double-logarithmic plots.[28]

The values of charge carrier mobility, calculated through the well-known expression $\mu = d/\tau E$ where d is the thickness of the polymer layer, are shown as a function of the applied electric field in Fig. 6. As far as the trend of μ with E is concerned, being the same for both positive and negative carriers for each AnE-PV*stat* sample, again the main difference was observed between AnE-PV*stat*-c and the other two polymer samples, both showing a higher overall degree of order as observed with XRD. It has already been reported that charge carrier mobility in AnE-PV*stat*-c films shows a Poole-Frenkel behaviour both for holes and electrons,[19] with an exponential increase of μ with the square root of E. Differently, mobility in AnE-PV*stat*-a and AnE-PV*stat*-b films exhibits a decreasing trend for low fields and reaches a minimum before starting increasing with E. The Poole-Frenkel-like trend of mobility is often observed for disordered organic materials, while behaviour similar to that exhibited by AnE-PV*stat*-a and AnE-

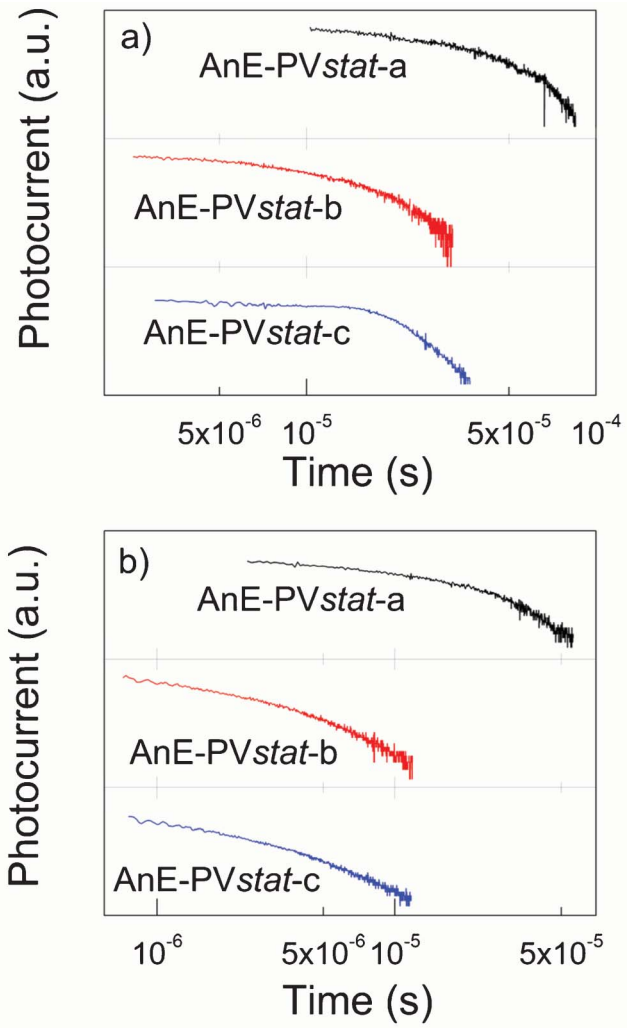

Fig. 5 Log-log plots of photocurrent signals for holes (a) and electrons (b) for a comparable electric field of about 1×10^5 V cm^{-1}.

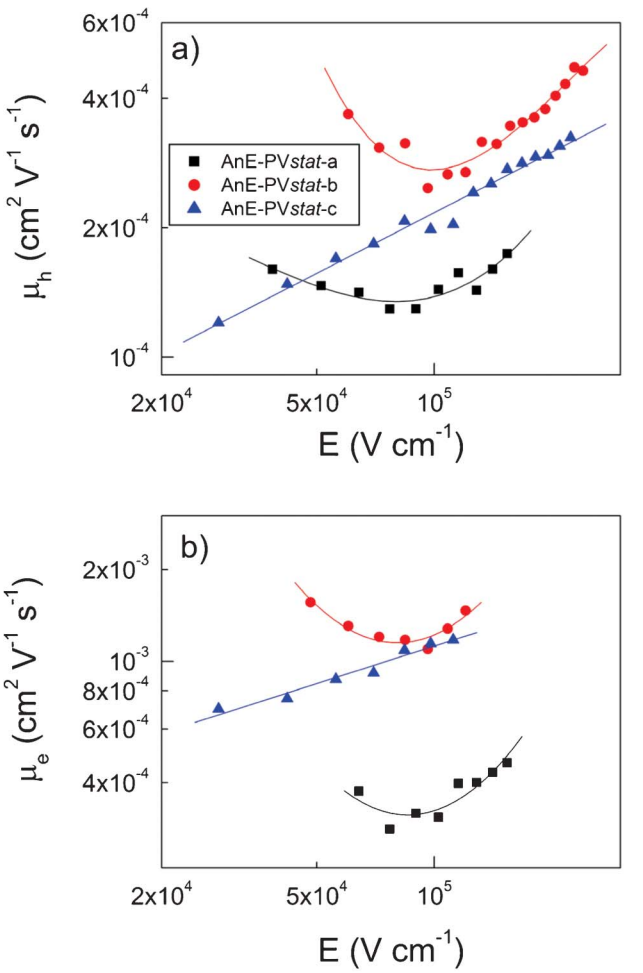

Fig. 6 Hole (a) and electron (b) drift mobility as a function of the applied electric field: AnE-PV*stat*-a (squares); AnE-PV*stat*-b (circles); AnE-PV*stat*-c (triangles). Lines are shown to guide the eye.

PV*stat*-b samples is less common. As an example, a decreasing trend of μ at low field is usually observed for regioregular poly(3-hexilthiophene).[29,30] Both types of trend exhibited by the mobility in the three AnE-PV*stat* samples can be explained within the same model of an hopping conduction in a Gaussian distribution of localized states, as demonstrated by Monte Carlo simulations.[31,32] Indeed, depending on the relative contribution of energetic (diagonal) and positional (off-diagonal) disorder to the random walk of charge carriers, a Poole-Frenkel-like behaviour or a change of sign of the field dependence of mobility can be observed. Interestingly, the minimum of μ is reached both for AnE-PV*stat*-a and AnE-PV*stat*-b at the same field value of about 10^5 V cm^{-1}, suggesting that the role of energetic and off-diagonal disorder is qualitatively similar for these two polymers samples showing higher polydispersity index. As already reported for sample AnE-PV*stat*-c,[19] AnE-PV*stat* shows a good ambipolar behaviour, with drift electron mobility even higher than that evaluated for holes (compare Fig. 6a with Fig. 6b), at least in the investigated field range. For both types of carriers, drift mobility shows a clear dependence on the macromolecular parameters. At low fields (below 5×10^4 V cm^{-1}), the hole mobility seems to be correlated to the mean domain length (Table 1), with more ordered polymer samples showing higher mobility. However hole mobility in sample AnE-PV*stat*-c surpasses that in sample AnE-PV*stat*-a as E is increased, because of the strong field activation of the less ordered polymer also at moderate electric fields.

In order to analyze the effect of the macromolecular parameters on the photovoltaic properties of AnE-PV*stat*, bulk heterojunction solar cells were prepared with the three polymer samples as electron-donors and PCBM as acceptor (PCBM is [6,6]-phenyl-C_{61}-butyric acid methylester). Since for a given donor/acceptor (D/A) pair, the maximum photovoltaic performance of the related blends is determined by a critical interplay between different factors, such as miscibility, deposition conditions, blend thickness, donor to acceptor ratio, pre- and/or post-treatments,[33] the comparison of different D/A pairs is not so straightforward. For this reason the aim of this work was not the optimization of solar cell devices, but to establish how the photovoltaic properties of

AnE-PV*stat*:PCBM blends were affected when an organization of the donor phase close to that of drop-casted thick films already investigated was induced. To this end, efforts were made to use deposition and treatment conditions able to induce such organization in spin-coated thin films, required for lab-scale solar cell preparation. The AnE-PV*stat*:PCBM active layers were deposited onto ITO/PEDOT:PSS substrates by using a not too high D/A ratio by weight (1 : 1), the same solvent chlorobenzene, the same solution concentration, the same low rotation speed of the spin-coater. After the deposition, the AnE-PV*stat*:PCBM films were solvent-vapor annealed for one hour, in order to foster the polymer chain organization through the slow-drying process.

The photovoltaic parameters of solar cells based on the three AnE-PV*stat* donors are collected in Table 2, along with the thickness of the active layers, while the related current–voltage characteristics are displayed in Fig. 7. A straight comparison can be done for the same active layer thickness. Solar cells made with AnE-PV*stat*-a show a slightly higher short-circuit current (J_{sc}) with respect to those with AnE-PV*stat*-b donor, which could arise from an increased A/D interface, leading to a slightly higher generation of charge carriers. This could be due to a more intimate mixing with the PCBM moiety because of the longer polymer chains of AnE-PV*stat*-a. However, the striking difference in the photovoltaic parameters of the two kinds of cells is given by fill factor (*FF*), raising from 0.46 for AnE-PV*stat*-a to 0.67 for AnE-PV*stat*-b, giving a strong indication of very different transport properties in the blends and confirming the mobility data. As expected,[34] the open-circuit voltage (V_{oc}) was not meaningfully affected by the donor component (Table 1) and the enhanced *FF* of AnE-PV*stat*-b based cells led to a power conversion efficiency (PCE) of 3.26%, to be compared with 2.38% of AnE-PV*stat*-a based cells. Concerning AnE-PV*stat*-c donor, the short circuit current, thus PCE, can hardly be compared with the values observed for the other solar cells, because of the reduced active layer thickness. However, some consideration can be done on fill factor, which, differently from J_{sc}, is not affected by the lower solar light harvesting ability of cells made with AnE-PV*stat*-c donor. Fill factor of AnE-PV*stat*-c cells was found to be 0.51, in between those of the other cells, again confirming the trend of hole mobility in pristine AnE-PV*stat* films (Fig. 6a). Fig. 8 shows the straight correlation between fill factor of solar cells and the mobility of positive carriers measured in pristine AnE-PV*stat* films at a field of about 1×10^5 V cm^{-1}.

Table 2 Active layer thickness and photovoltaic parameters (AM1.5G, 100 mW cm^{-2}) of solar cells made with AnE-PV*stat* donors and PCBM acceptor in 1 : 1 weight ratio

	Thick (nm)	J_{sc} (mA cm^{-2})	V_{oc} (V)	*FF*	PCE (%)
AnE-PV*stat*-a	135	6.10	0.85	0.46	2.38
AnE-PV*stat*-b	130	5.57	0.87	0.67	3.26
AnE-PV*stat*-c	93	3.82	0.89	0.51	1.73

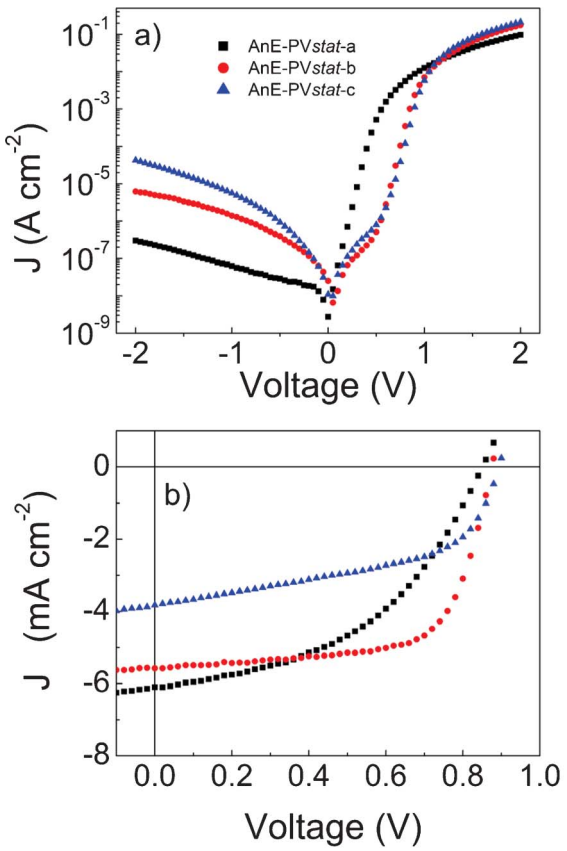

Fig. 7 Current density–voltage characteristics in the dark (a) and under 100 mW cm^{-2} illumination (b) for solar cells made with the three electron-donors: AnE-PV*stat*-a (squares); AnE-PV*stat*-b (circles); AnE-PV*stat*-c (triangles).

4. Conclusions

A variation of just a factor of around two in the molecular weight of AnE-PV*stat* led to appreciable modifications in the optical, morphological, and transport properties of its films,

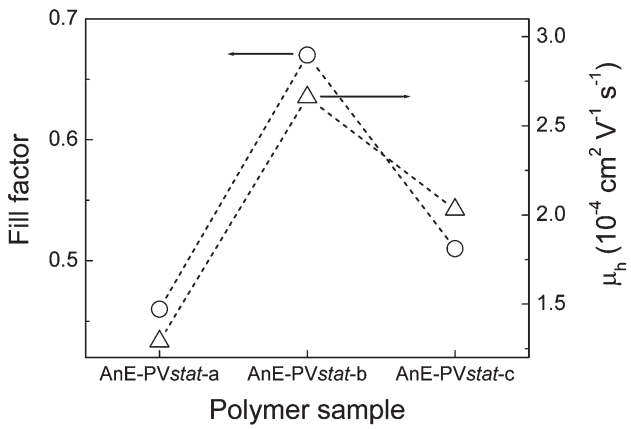

Fig. 8 Fill factor of AnE-PV*stat*:PCBM solar cells (left, circles) and TOF hole mobility, at about 1×10^5 V^{-1} cm^{-1}, of pristine AnE-PV*stat* films (right, triangles).

reflecting in the behaviour of AnE-PV*stat*:PCBM solar cells. Not only the mobility data were affected by the macromolecular parameters, but also the trend of μ with the applied electric field. A Poole-Frenkel-like behaviour was obtained for less ordered AnE-PV*stat*-c films, while a minimum of μ at around 1×10^5 V^{-1} cm^{-1} was observed for the other two polymer samples giving more ordered arrangements in cast-films. A strong correlation between the fill factor of AnE-PV*stat*:PCBM solar cells and the mobility of pristine AnE-PV*stat* films was obtained, suggesting that the tuning of the donor macromolecular parameters is critical for high performance polymer/fullerene solar cells.

The comparison of AnE-PV*stat*-a and AnE-PV*stat*-c, showing the same peak in the GPC curves but different PDI, indicated that polydispersity plays a significant role in the organization of polymer chains in the investigated films, thus affecting all their properties.

This study clearly demonstrates the importance of the fine tuning of the macromolecular parameters for the electronic properties of conjugated polymers.

Acknowledgements

This work was partly supported by ENI S.p.A. (contract n. 4700007315). D. A. M. Egbe acknowledges the Deutsche Forschungsgemeinschaft (DFG) for the financial support in the framework of the priority program SPP1355. V. Cimrova acknowledges for the financial support of the Grant Agency of the Czech Republic (grant No. 13-26542S and P106/12/0827). F. K. Sabir acknowledges the Abdus Salam International Centre for Theoretical Physics (ICTP) for financial support in the framework of the "Programme for Training and Research in Italian Laboratories (TRIL)".

References

1 *Printed Organic Molecular Electronics*, ed., D. R. Gamota, P. Brazis, K. Kalyanasundaram and J. Zhang, Kluwer Academic, Norwell, 2004.
2 A. J. Heeger, *Chem. Soc. Rev.*, 2010, **39**, 2354.
3 M. T. Lloyd, J. E. Anthony and G. G. Malliaras, *Mater. Today*, 2007, **10**, 34.
4 A. Yassin, T. Rousseau, P. Leriche, A. Cravino and J. Roncali, *Sol. Energy Mater. Sol. Cells*, 2011, **95**, 462.
5 M. Brinkmann and P. Rannou, *Adv. Funct. Mater.*, 2007, **17**, 101.
6 S. Joshi, S. Grigorian and U. Pietsch, *Phys. Status Solidi A*, 2008, **205**, 488.
7 A. Facchetti, *Chem. Mater.*, 2011, **23**, 733.
8 R. J. Kline, M. D. McGehee, E. N. Kadnikova, J. Liu and J. M. J. Fréchet, *Adv. Mater.*, 2003, **15**, 1519.
9 A. Zhen, M. Saphiannikova, D. Neher, J. Grenzer, S. Grigorian, U. Pietsch, U. Asawapirom, S. Janietz, U. Scherf, I. Lieberwirth and G. Wegner, *Macromolecules*, 2006, **39**, 2162.
10 J.-M. Verilhac, G. LeBlevennec, D. Djurado, F. Rieutord, M. Chouiki, J.-P. Travers and A. Pron, *Synth. Met.*, 2006, **156**, 815.
11 A. M. Ballantyne, L. Chen, J. Done, T. Hammant, F. M. Braun, M. Heeney, W. Duffy, I. McCulloch, D. D. C. Bradley and J. Nelson, *Adv. Funct. Mater.*, 2008, **18**, 2373.
12 R. C. Hiorns, R. de Bettignies, J. Leroy, S. Bailly, M. Firon, C. Sentein, A. Khoukh, H. Preud'homme and C. Dagron-Lartigau, *Adv. Funct. Mater.*, 2006, **16**, 2263.
13 P. Schilinsky, U. Asawapirom, U. Scherf, M. Biele and C. J. Brabec, *Chem. Mater.*, 2005, **17**, 2175.
14 W. Ma, J. Yo. Kim, K. Lee and A. J. Heeger, *Macromol. Rapid Commun.*, 2007, **28**, 1776.
15 M. Tong, S. Cho, J. T. Rogers, K. Schmidt, B. B. Y. Hsu, D. Moses, R. C. Coffin, E. J. Kramer, G. C. Bazan and A. J. Heeger, *Adv. Funct. Mater.*, 2010, **20**, 3959.
16 J.-M. Verilhac, R. Pokrop, G. LeBlevennec, I. Kulszewicz-Bajer, K. Buga, M. Zagorska, S. Sadki and A. Pron, *J. Phys. Chem. B*, 2006, **110**, 13305.
17 Ö. Usluer, C. Kästner, M. Abbas, C. Ulbricht, V. Cimrova, A. Wild, E. Birckner, N. Tekin, N. S. Sariciftci, H. Hoppe, S. Rathgeber and D. A. M. Egbe, *J. Polym. Sci., Part A: Polym. Chem.*, 2012, **50**, 3425.
18 (*a*) P. A. Troshin, O. A. Mukhacheva, Ö. Usluer, A. E. Goryachev, A. V. Akkuratov, D. K. Susarova, N. N. Dremova, S. Rathgeber, N. S. Sariciftci, V. F. Razumov and D. A. M. Egbe, *Adv. Energy Mater.*, 2013, **3**, 161; (*b*) C. Kästner, C. Ulbricht, D. A. M. Egbe and H. Hoppe, *J. Polym. Sci., Part B: Polym. Phys.*, 2012, **50**, 1562.
19 N. Camaioni, F. Tinti, A. Degli Esposti, S. Righi, Ö. Usluer, S. Boudiba and D. A. M. Egbe, *Appl. Phys. Lett.*, 2012, **101**, 053302.
20 R. Jadhav, S. Türk, F. Kühnlenz, V. Cimrova, S. Rathgeber, D. A. M. Egbe and H. Hoppe, *Phys. Status Solidi A*, 2009, **12**, 2695.
21 D. A. M. Egbe, S. Türk, S. Rathgeber, F. Kühnlenz, R. Jadhav, A. Wild, E. Birckner, G. Adam, A. Pivrikas, V. Cimrova, G. Knör, N. S. Sariciftci and H. Hoppe, *Macromolecules*, 2010, **43**, 1261.
22 S. Rathgeber, D. Bastos de Toledo, E. Birckner, H. Hoppe and D. A. M. Egbe, *Macromolecules*, 2010, **43**, 306.
23 D. A. M. Egbe, G. Adam, A. Pivrikas, A. M. Ramil, E. Birckner, V. Cimrova, H. Hoppe and N. S. Sariciftci, *J. Mater. Chem.*, 2010, **20**, 9726.
24 S. Rathgeber, J. Perlich, F. Kühnlenz, S. Türk, D. A. M. Egbe, H. Hoppe and R. Gehrke, *Polymer*, 2011, **52**, 3819.
25 D. A. M. Egbe, B. Carbonnier, E. Birckner and U.-W. Grummt, *Prog. Polym. Sci.*, 2009, **34**, 1023.
26 H. P. Klug and L. E. Alexander, *X-ray diffraction procedures for polycrystalline and amorphous materials*, John Wiley, New York, 2nd edn, 1974.
27 P. M. Borsenberger and D. S. Weiss, *Organic Photoreceptors for Xerography*, Marcel Dekker, New York, 1998.
28 H. Scher and E. W. Montroll, *Phys. Rev. B: Solid State*, 1975, **12**, 2455.
29 S. A. Choulis, Y. Kim, J. Nelson, D. D. C. Bradley, M. Gilles, M. Shkunov and I. McCulloch, *Appl. Phys. Lett.*, 2004, **85**, 3890.
30 V. Kažukauskas, M. Pranaitis, V. Čyras, L. Sicot and F. Kajzar, *Eur. Phys. J.: Appl. Phys.*, 2007, **37**, 247.

31 L. Pautmeier, R. Richert and H. Bässler, *Synth. Met.*, 1990, **37**, 371.
32 P. M. Borsenberger, L. Pautmeier and H. Bässler, *J. Chem. Phys.*, 1991, **94**, 5447.
33 G. Li, R. Zhu and Y. Yang, *Nat. Photonics*, 2012, **6**, 153.
34 C. J. Brabec, A. Cravino, D. Meissner, N. S. Sariciftci, T. Fromherz, M. T. Rispens, L. Sanchez and J. C. Hummelen, *Adv. Funct. Mater.*, 2001, **11**, 374.

